Adhesive-based liquid metal radio-frequency microcoil for magnetic resonance relaxometry measurement

Kong, Tian Fook; Peng, Weng Kung; Luong, Trung-Dung; Nguyen, Nam-Trung; Han, Jongyoon

2012

Kong, T. F., Peng, W. K., Luong, T. D., Nguyen. N.-T. & Han J. (2012). Adhesive-based liquid metal radio-frequency microcoil for magnetic resonance relaxometry measurement. Lab on a Chip, 12, 287-294.

https://hdl.handle.net/10356/94441

https://doi.org/10.1039/C1LC20853E

Adhesive-based liquid metal radio-frequency microcoil for magnetic resonance relaxometry measurement

Tian Fook Kong, [a,b] **Weng Kung Peng,** [b] **Trung Dung Luong,** [a] **Nam-Trung Nguyen,** [*a,b] **Jongyoon Han,** [*b,c,d]

Abstract

This paper reports the fabrication and characterization of an adhesive-based liquid-metal microcoil for magnetic resonance relaxometry (MRR). Conventionally, microcoils are fabricated by various techniques such as electroplating, microcontact printing and focused ion beam milling. These techniques require considerable fabrication efforts and incur high cost. In this paper, we demonstrate a novel technique to fabricate three-dimensional multilayer liquid-metal microcoils together with the microfluidic network by lamination of dry adhesive sheets. One of the unique features of the adhesive-based technique is that the detachable sample chamber can be disposed after each experiment and the microcoil can be reused without cross-contamination for multiple times. The integrated microcoil has a low direct-current (DC) resistance of 0.3 Ω and a relatively high inductance of 67.5 nH leading to a high quality factor of approximately 30 at 21.65 MHz. The microcoil was characterized for 0.5 T proton MRR measurements. The optimal pulse duration, amplitude, and frequency for the 90° pulse were 131 μs, -30 dB (1.56 W) and 21.6553 MHz, respectively. In addition, we used the liquid-metal microcoil to perform a parametric study on the transverse relaxation rate of human red blood cells at different hematocrit levels. The transverse relaxation rate increases quadratically with the hematocrit level. The results from the liquid-metal microcoil was verified by measurements with a conventional solenoid coil.

Introduction

In recent years, labs on a chip (LOC) or micro total analysis systems (μTAS) have been the main sources of innovation for microfluidic technology. In the past, many biological applications requiring an integrated metal conductor such as microcoils and microstriplines have been reported. The applications of these conducting structures include magnetic cell sorting,[1] immunoassay,[2] and deoxyribonucleic acid (DNA) purification.[3] One important research area that needs microcoil with a high degree of geometric precision and reproducibility is nuclear magnetic resonance (NMR) detection.[4]

[a] *School of Mechanical and Aerospace Engineering, Nanyang Technological University, 50 Nanyang Avenue, 639798 Singapore. E-mail: mntnguyen@ntu.edu.sg*

[b] *BioSystems and Micromechanics (BioSyM) IRG, Singapore-MIT Alliance for Research and Technology (SMART) Centre, S16-07, 3 Science Drive 2, 117543 Singapore. E-mail: jyhan@mit.edu*

[c] *Department of Electrical Engineering & Computer Science, Massachusetts, Institute of Technology, Room 36-841, 77 Massachusetts Avenue, Cambridge, MA, USA*

[d] *Department of Biological Engineering, Massachusetts Institute of Technology, Cambridge, MA, USA*

The integration of microfabricated microcoil in a NMR system for bio-sensing has attracted a great interest from the NMR research community. The main motivations behind such interest are the technical challenges associated with the high strength, spatially uniform magnetic field, which is necessary for conventional NMR measurement. Although NMR sensitivity increases with the magnetic field strength[5], a highstrength homogeneous magnetic field is expensive, bulky, and difficult to maintain. Furthermore, the miniaturization of a NMR system offers a higher mass sensitivity and requires a smaller sample volume.[6,7] Microdetectors for magnetic resonance-based applications were realized by various coil configurations such as the micro stripline probe,[8] microslot waveguide,[9] and wirebonded microcoil.[10] The recently developed palm-sized NMR system[11] demonstrated the feasibility and potential of a miniature magnetic resonance system for point-of-care diagnosis.[12] These miniaturized NMR systems hold great promises as biomarker detectors for disease and cancer screening.[13,14] We have recently shown that the presence of paramagnetic particles in parasites infected red blood cells gives rise to relaxation contrast, which can be used as a natural biomarker in disease diagnosis such as malaria.[15–17] With our bench-top magnetic resonance relaxometry (MRR) system, the assay was performed on less than 1 μL whole blood with detection time of less than 1 minute.

With advanced micromachining technologies, the focus has been shifted to the batch fabrication of microcoil using standard photolithography processes such as thermal/ebeam evaporation;[1] electroplating;[18] printed circuit board (PCB) etching;[19,20] microcontact printing;[21] and focused ion milling.[22] However, the shortcomings of the above techniques are as follow. Thermal/e-beam evaporation has low material deposition rate and cannot achieve high-aspect-ratio metal structures. Electroplated metal structures are porous and have rough surface finishes. Etching PCB has limited resolution due to the isotropic nature of the wet etchant. Microcontact printed film has high contact resistance. Focused ion milling technique is a serial technique and incurs high fabrication cost.

The introduction of microsolidics, a fabrication method for multi-layered three-dimensional (3D) metallic structures in microchannels,[23] has revolutionized how metallic conductors are integrated in the LOC platform. The key advantage of using liquid-metal technology is the ability of making flexible complex 3D electrical conductors, confined in a microchannel, with only few fabrication steps. The liquidmetal structures are mechanically deformable allowing applications such as tunable fluidic antenna,[24,25] pressure sensor,[26] aligned microfluidic electrodes for electrophoresis,[27] and conical tip conformal electrodes for studying the charge transport across self-assembled monolayers.[28] Recently Lam et. al. demonstrated the fabrication of microcoil by injection of liquid metal into a solenoidal microchannel.[29] However, the softlithography fabricated solenoidal microcoil has limited sensitivity and resolution due to the low conductivity and magnetic susceptibilities mismatch of the construction materials. Furthermore, the electrical contacts made between the coil and the NMR probe by inserting copper wires gives high contact resistance and are usually unstable.

In this paper, we present a novel technique for the fabrication of three-dimensional multilayer liquid-metal microcoils together with the microfluidic network by lamination of dry adhesive sheets. As the adhesive sheet readily bonds to a

PCB, we achieved a firm and stable contact between the liquid metal coil and the metal contact pads on the PCB, thus ensuring an excellent electrical contact between the coil and external devices. Our liquid-metal microcoil has the highest quality factor among the NMR microcoils published previously. [6,7,11,22] With the lamination approach, the microcoil readily integrates with the sample chamber MRR measurements. Another unique feature of the adhesive-based technique is that the detachable sample chamber can be disposed after each measurement without affecting the microcoil assembly. Therefore, the microcoil can be reused for multiple measurements. Unlike conventional microfabrication methods, there is no need for cleaning the sample chamber before every measurement and the cross-contamination issue between different samples is eliminated. We focus the current study on characterizing the adhesive-based liquid-metal microcoil for 21.65 MHz proton (^{1}H) MRR measurements in a permanent magnet of 0.5 T. In addition, we performed a parametric study on the relationship between the transverse relaxation rate R_2 and the hematocrit level of human red blood. The results of the R_2-hematocrit level relationship obtained by the liquid-metal microcoil are compared with those from a conventional solenoid coil.

Materials and methods

Device fabrication

The integrated liquid-metal NMR device consists of two major components: a microcoil and a sample chamber. The fabrication of the integrated device was realized by laminating multiple layers of laser-cut adhesive sheets (Arclad ® 5913 Adhesives Research Inc., USA). The adhesive sheet is a polyester film double-coated with acrylic adhesive. One of the major advantages of using the stacking approach is that the layers can be fabricated easily by laser machining, without the need of photolithography and cleanroom access. Fig. 1 (a) shows the schematic diagram of the stacking approach for the fabrication of a multilayer NMR device. The layouts were designed in Autocad (Autodesk, USA) and sent to a laser cutting machine (M300, Universal laser systems Inc., USA) for fabrication. The laser machine cut the 75-μm adhesive sheet into individual layers of the microcoil and sample chamber. These individual layers were then aligned and assembled into an integrated lab-on-chip NMR sensing device. The integrated device with the liquid-metal microcoil and the sample chamber was attached to the bottom part of a NMR probe. The probe was subsequently placed inside a 0.5-T

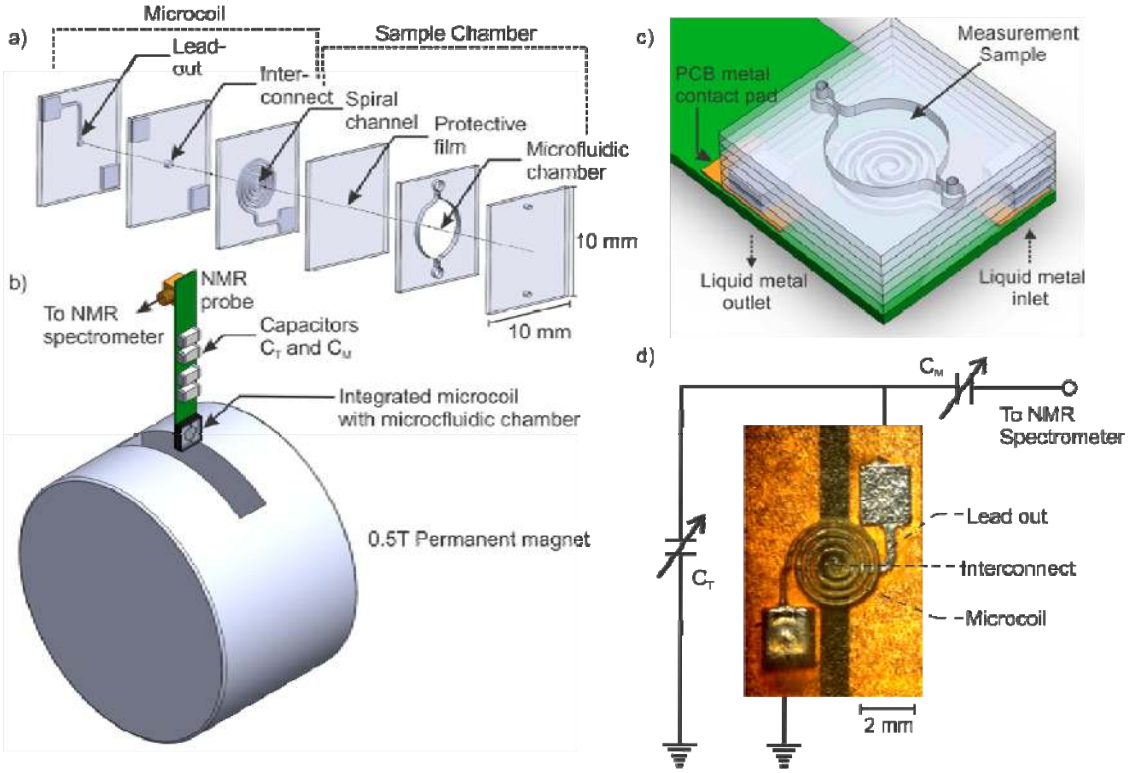

Figure 1: (a) Schematic diagram of the stacking approach for the fabrication of a multilayer integrated NMR microcoil and the sample chamber. The microcoil consists of three layers: (i) the spiral channel; (ii) the interconnect; and (iii) the lead-out channel, while the sample chamber is placed directly on top of the assembled microcoil for MRR measurements. The required sample volume is 5 μL and can be disposed and replaced without affecting the microcoil. (b) The integrated patch of the liquid-metal microcoil and microfluidic chamber is attached to the bottom part of the NMR probe. The probe is placed inside a 0.5 T permanent magnet. (c) Schematic diagram for the assembled MRR device. The large contact areas between the PCB metal contact pads and liquid metal ensures low contact resistance between the microcoil and the external device (NMR probe). (d) A simple L-network for matching the microcoil impedance to 50 Ω and tuning the resonance frequency of the coil to 21.65 MHz for 0.5 T proton magnetic relaxometry measurements. Electrical signal passes through from the spiral coil to the bottom lead out channel through a middle interconnect layer. Misalignment between these three layers would cause an open circuit. The typical resistance of a planar microcoil with both width and gap of 250 μ m is approximately 0.3 Ω .The probe is connected to a NMR spectrometer via a RF coaxial cable.

permanent magnet for MRR measurements, Fig. 1(b).

The microcoil structure consists of three layers: the spiral channel, the interconnect and the lead-out channel. The microcoil investigated in this paper has five turns ($n = 5$) and a feature size of 250 μm for both coil width and gap. Liquid metal, gallium (Sigma-Aldrich, USA) was first injected through the spiral coil, then passed through the middle interconnect layer, and finally exited via the lead-out channel. Fig. 2.1 (d) shows the optical micrograph of an assembled microcoil filled with liquid gallium. Since gallium has a low melting point of 29.8 $^\circ$C, it melts when subjected to heat and could easily be injected manually into the microchannel embedded in the adhesive sheets.

The microcoil was then cooled at room temperature for one hour to allow sufficient time for liquid gallium to solidify. While the electrical resistivity of gallium at 20 $^{\circ}C$ is 270 n $\Omega \cdot$m, the direct-current (DC) resistance of the multilayered planar microcoil is typically about 0.3 Ω as measured with a multimeter (Fluke 175). However, if the interconnect layer is misaligned with the spiral and lead-out layers, the coil will either have a high contact resistance become an open circuit.

With the help of four poles made of G15 blunt-head needles (Nordson EFD Inc., USA), the adhesive layers with 2-mm alignment holes at the four corners can be precisely aligned and bonded. The alignment accuracy was approximately 50 to 100 μm. Five sheets of adhesive, each of which was 75 μm thick were bonded together prior to laser cutting to achieve to achieve a high-aspect-ratio microcoil. In this way, a coil thickness of 375 μm was achieved. If the laser cut through the adhesive layer of the spiral channel, the resulting spring-like spiral structure was not supported and difficult to handle. Thus, it is crucial to optimize the laser cutting power and speed such that the laser engraves down to about 95 % of the layer thickness, leaving a thin membrane for supporting the spiral channel.

Another area where adhesive-based liquid-metal microchannel would excel over that made in polydimethylsiloxane (PDMS) channel is the ability of making a low-contact-resistance electrical connection to an external device. Conventionally, metal pins or wires are inserted into the PDMS inlet to realize the electrical interconnects. Since the contact areas between the metal pins or wires are small, the contact resistance is usually high and unstable. In contrast, since the adhesive sheet readily bonds to a PCB, we are able to achieve a firm and stable contact between the contact pads on the PCB and the liquid metal. First, the inlets and outlets of the adhesive coil are designed so that the inlets and outlets are located on top of the PCB metal pads. Through-holes of 1-mm diameter were mechanically drilled on the contact pads of the PCB. The assembled microcoil was then attached to the PCB with the inlet and outlets aligned on top of the PCB contact pads, Fig. 1(c). Next, liquid metal was injected from the back of the PCB, making the liquid metal flows through the first copper pad on the PCB, into the spiral channel. The liquid metal flows through the interconnect layer, followed by the lead-out channel back to the other PCB contact pad and finally exits through the drilled outlet on the PCB. The large contact area between the liquid metal and the PCB contact pads ensure an excellent electrical connection to external devices. The overall resistance of the liquid metal microcoil is 0.3 Ω, while the resistance with metal pin or wire connectors is in the order of several tens to thousands Ohm.

The sample chamber consists of a cut-through circular chamber sealed with an adhesive sheet and a protective film at the top and the bottom, respectively. The fluidic chamber is placed directly on top of the assembled microcoil for NMR detection and measurements. Since the protective film that come with the adhesive does not adhere permanently to the adhesive sheet, it can be used as a separation layer between the microcoil and the sample chamber. The sample chamber can be disposed and replaced for measuring different samples. This concept ensures that there is no cross contamination between different samples and there is no need to clean the sample chamber before every measurement. The ability to replace the sample chamber eliminates the need of fabricating a new liquid-metal microcoil and re-perform the tuning and matching for the NMR probe when measuring different samples. The total sample volume of the our

device is 5 μL.

In this work, we focused on the characterization of planar microcoil for MRR applications. The fabrication technique of the adhesive-based liquid metal microcoil described in this section could be extended for more complex three-dimensional coil geometries such as the solenoid and saddle microcoil.

Experimental setup

The integrated liquid-metal microcoil was used as the receiver for MRR measurements. A simple L-network configuration was used for matching the microcoil impedance to 50 Ω and tuning the resonance frequency of the coil to 21.65 MHz for 0.5 T proton magnetic relaxometry measurements. First, the probe resonance frequency was adjusted with capacitor C_{T}. As observed with a radio-frequency (RF) sweeper (405NV+, Morris Instruments Inc., Canada), the probe resonance frequency decreases with increasing capacitance of C_{T}. Subsequently, the capacitance value of C_{M} was varied to match the probe impedance to the standard 50 Ω. The typical values of the tuning and matching capacitance for the five-turn microcoil with a width of 250 μm are 1000 pF and 220 pF, respectively. A schematic diagram for the L-network is shown in Fig. 1(d). Maximum power transfer to and from the NMR probe occurs when the load impedance is the complex conjugate of the source impedance.[30] The probe was placed in a 0.5 T NMR permanent magnet (PM-1055, Metrolab Instruments, Switzerland) during the measurements. The probe was then connected via a RF coaxial cable to a commercial bench-top NMR spectrometer (KEA2, Magritek, New Zealand) with a maximum power output capacity of 100 W. The MRR measurements were carried out with a software (Prospa v2.0) provided by the system manufacturer.

Sample Preparation

Blood samples at various hematocrit levels were prepared by mixing normal human red blood cell (RBC) with phosphate buffered saline (PBS 1 X) pH 7.4 without calcium chloride or magnesium chloride (17-516Q, Lonza Walkersville, Inc., USA) at different volume ratios under room temperature. The RBCs were drawn from healthy human volunteer. The total blood volume (after mixing) required for each measurement was 20 μL, with 15 μL being used for hematocrit level measurement and the remaining 5 μL for the MRR measurements. The blood sample was pipetted repeatedly on a piece of glass slide to ensure the blood has been saturated with oxygen. The actual hematocrit level of the blood sample is determined by centrifugation. First, a 15-μL blood sample was drawn into a microcapillary tube with volume of 20 μL, an outer diameter of 900 μm, and an inner diameter of 550 μm (Drummond Scientific Co., USA) by capillary filling. Subsequently, one end of the microcapillary tube was sealed with a vinyl-plastic compound (Critoseal, Krackeler Scientific, USA). The blood sample was then centrifuged at 6,000 g for 5 minutes in a microcentrifuge machine (Sorvall Legend Micro 21, Thermo Scientific, USA). The hematocrit level (or the packed cell volume) of the blood sample was determined as the ratio between the height of the red blood cell column and the total height of the blood column. The systematic error of the

hematocrit measurement was derived from error propagation analysis.

3. Results and discussion

3.1 Microcoil Characterization

The integrated adhesive-based liquid-metal microcoil was characterized for ^{1}H proton MRR measurements at 0.5 T. The sample used for the results in Fig. 2 was human blood with approximately 40 % hematocrit. The effective observed volume for the microcoil is 942 nL (diameter of 4 mm and height of 150 μm). First, the tuning and matching capacitance C_{T} and C_{M} were adjusted such that the minimum amount of RF energy reflected from the probe occurs at 21.65 MHz, corresponding to a 0.5 T Larmor frequency. We run the macro function provided by the software Prospa to measure the amount of RF energy reflected from the probe. Ideally, if the probe is tuned and matched to 50 Ω, the amount of RF energy reflected should be zero.

Table 3.1: Comparison of liquid-metal microcoil with other coils fabricated with other techniques as reported in the literature (coil type, inner diameter D_i, number of turns N, inductance L, resistance R, frequency f, and quality factor Q)

Reference	**Coil Type**	D_i (μm)	**N (turns)**	**L (nH)**	**R** (Ω)	**f (MHz)**	**Q**
This work	planar spiral	500	5	67.48	0.3	21.65	30.4
Massin et. al.[6]	planar spiral	500	3	8.7	0.7	300	23.5
Sun et. al.[11]	planar spiral	-	25	430	31	20.9	1.9
Hsieh et. al.[7]	Saddle	500	2	-	0.7	200	15
Sillerud et. al.[22]	Solenoid	400	28	93	5.4	44.2	10

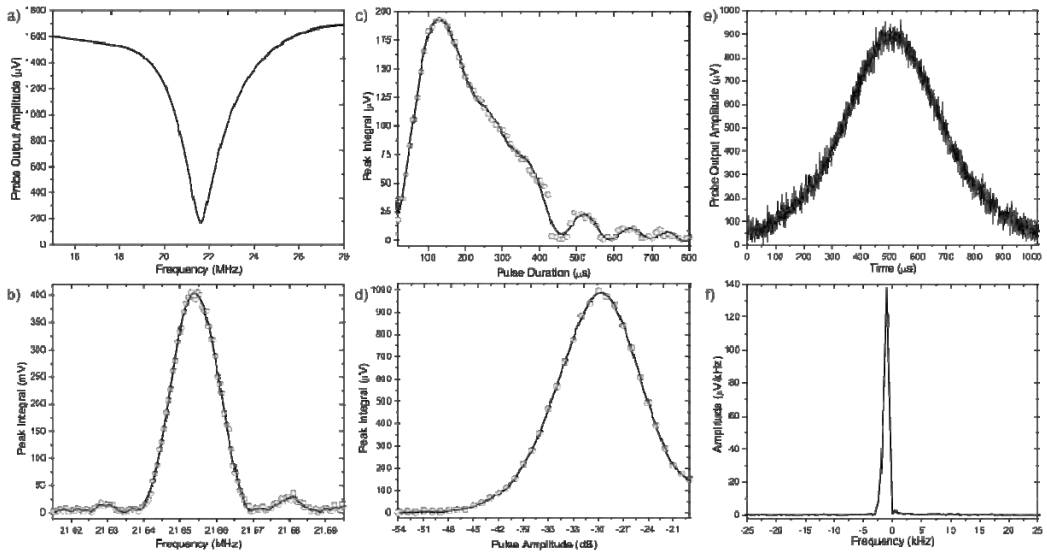

Figure 2: Characterization of the liquid-metal microcoil for ^{1}H MRR measurement: (a) The tuning and matching capacitance are adjusted such that the minimum amount of RF energy reflected from the probe occurs at 21.65 MHz, corresponding to a 0.5 T proton MRR resonance frequency. (b) The peak integral obtained by the Fourier transformation of the collected echo-sum for a range of frequency from 21.615 MHz to 21.695 MHz. The optimal NMR resonant frequency, at which the peak integral is maximum, is 21.6553 MHz. (c) The 90° pulse duration required to rotate the magnetic moment into the transverse plane is 131 μs. (d) The pulse amplitude is varied from -54 dB to -19 dB to find the optimal 90 and 180 degree pulses. The required power for the 90° pulse is -30 dB or 1.56 W. (e) CPMG spin-echo obtained with 5 ms echo time and 24 scans. (f) Magnitude spectrum of the CPMG spin-echo in acquired in (e).

However, in the actual experimental conditions, the minimum output amplitude of the probe is 172 μV at 21.65 MHz, Fig. 2(a).

In order to find the optimal MRR resonant frequency, a spin-echo experiment was carried out for a range of frequency from 21.615 MHz to 21.695 MHz. The Carr-Purcell-Meiboom-Gill (CPMG) peak integral obtained by the Fourier transformation of the collected echo-sum across the frequency range is shown in Fig. 2(b). The optimal MRR resonant frequency, at which the peak integral is maximum, is at 21.6553 MHz. The parameters used were 4 scans, 110 μs pulse duration, 2000 echoes, 2 ms echo time, 5 s repetition time, 21.6553 MHz B_0, -36 dB (1.5625 W) 90° pulse and -30 dB (3.125 W) 180° pulse. In addition, we performed a frequency sweep for the microcoil with no sample loaded to examine if the adhesive and protective layers give a background MRR signal. The peak integrals across the range of frequency are simply random noise with the root-mean-square value of 5.14 mV (figure not shown). Hence, the problem of background signal from the adhesive and protective layer does not exist. With the maximum peak integral of 404 mV obtained at 21.6553 MHz for blood sample, the signal to noise ratio of the microcoil is approximately 80.

The CPMG peak integral obtained for a pulse duration sweep of 21 to 800 μs is shown in Fig. 2(c). The 90° pulse duration required to rotate the magnetic moment into

the transverse plane is 131 μs. The asymmetry in the nutation performance curve could be caused by the inhomogeneous magnetic and RF field. The parameters used were 24 scans, 1000 echoes, 2 ms echo time, 5 s repetition time, 21.6553 MHz B_0, -36 dB 90° pulse and -30 dB 180° pulse.

The pulse amplitude was varied from -54 dB to -19 dB to find the optimal 90° and 180 ° pulses (48 scans, 1000 echoes and 1 ms echo time). The optimal power for the 90° pulse is -30 dB or 1.56 W, Fig. 2(d). The microcoil is able to withstand up to -18dB of power input (approximately 6.25W or a current of 4.56 A) before becoming an open circuit. Some areas of the liquid gallium coil channel become voids due to Joule heating, thus interrupting the electrical current. However, owing to the unique nature of the liquid-metal microcoil, the damaged coil could be repaired by reflowing of liquid metal in the coil channel. Coil heating is not an issue while performing CPMG MRR measurements since the applied pulse duration is short (131 μs) and the required 90° pulse amplitude (1.56 W) is much lower than the maximum power sustainable by the microcoil (6.25 W). Furthermore, the interval between pulses is kept sufficiently long (5 s), which gives a low RF duty cycle of less than 10 %. For an MRR experiment of about 10 hours, we did not observe any noticeable change in the measured longitudinal and transverse relaxation time (data not shown).

Fig. 2(e) shows the CPMG spin-echo obtained with 24 scans, 200 echoes, 5 ms echo time, 120 μs pulse duration, 5 s repetition time, 21.6553 MHz B_0, -36 dB 90° pulse and -30 dB 180° pulse, while Fig. 2 (f) shows the magnitude spectrum of the CPMG spin-echo in acquired in Fig. 2(e). The full-width-at-half-maximum line width of the frequency spectrum is 1.03 kHz or 47.58ppm. The relatively large line width is a result of inhomogeneous magnetic field, as no shimming was performed prior to the MRR measurements. However, as CPMG pulse sequence is insensitive to field inhomogeneity,[31] the line width of the frequency spectrum is not particularly important for MRR measurements. The line width could be further improved by performing shimming on the permanent magnet.

The inductance and quality factor are two important parameters that characterize a microcoil. The inductance, L of a circular planar coil can be estimated by the coil geometries using the following equation:[6,32]

$$L = 14\times10^{-7} N^2 \frac{(r_o + r_i + w)^2}{2.14 r_o - r_i + 0.57 w}, \quad (1)$$

where N is the number of turns, r_o is the outer coil radius, r_i is the inner coil radius, and w is the coil width. Hence, for a microcoil with $N = 5, r_o = 2000\,\mu$m, $r_i = 500\,\mu$m, and $w = 250\,\mu$m, the inductance of the integrated liquid-metal coil is calculated to be 67.5 nH.

A coil is deemed to have high quality factor if the energy loses are small compared to the total energy of the system. The quality factor, Q of the microcoil is given by: [6,22]

$$Q = \frac{\omega L}{R}, \quad (2)$$

where ω is the angular frequency, L is the coil inductance, and R is the resistance

of the coil. For 21.65MHz ^{1}H MRR measurements, the quality factor of the coil is estimated to be 30.4.

Table 3.1 compares the important parameters of our coil with those fabricated with other techniques as reported in the literature. Sun et. al.[11] attributed the low quality factor of its planar microcoil to the high DC resistance of 31 Ω. Similar drawback is also experienced by the solenoid-type microcoil fabricated with focused ion beam technology by Sillerud et. al.[22] due to the thin evaporated gold layer of 5 μm. As described in the device fabrication section, the liquid-metal microcoil reported in this paper has a DC resistance of only 0.3 Ω. Due to its relatively high inductance and low coil resistance, our liquid-metal microcoil achieves the highest quality factor among the NMR microcoils listed in Table 3.1.

3.2 ^{1}H MRR Measurements

The longitudinal (or spin-lattice) relaxation time, T_1 is the time constant for the exponential decay of the net magnetization to the equilibrium position after excited by a 90° pulse, while the transverse (or spin-spin) relaxation time, T_2 is the time constant that characterizes the dephasing of nuclei magnetic moment due the intrinsic molecular differences and inhomogeneities in the magnetic field.[33] Fig. 3 (a) shows the corrected echo integral collected with a standard inversion-recovery CPMG pulse sequence for deionized (DI) water. The T_1 relaxation time is 2520 ± 60 ms with 48 scans, 500 μs echo time, and 1000 echoes. Fig. 3 (b) shows echo integral collected with CPMG pulse trains. The T_2 relaxation time for DI-water is 2040 ± 10 ms with 48 scans, 1 ms echo time, and 3000 echoes. From the longitudinal and transverse relaxation time measurements shown in Fig. 3, the ability of the liquid-metal microcoil in performing MRR measurements is demonstrated.

3.3 Hematocrit-R_2 relationship for human red blood cell

Anemia is a medical condition where the red blood cell count or the quantity of hemoglobin in the body is low. Since one of the main functions of RBC is carrying oxygen from the lung to other parts of the body, low RBC count could lead to anemia hypoxia (lack of oxygen) and could be lethal.[34] With the ability to detect the subtle change in the blood hematocrit level, a portable MRR device could be developed to aid the diagnosis of anemia due to low red blood cell count. Current methods used for the determination of blood hematocrit level includes centrifugation, ultrasound,[35] and optical method.[36] Here, we performed a parametric study on the transverse relaxation rate of human red blood cell at different hematocrit levels using the liquid-metal microcoil. The transverse relaxation rate, R_2 is simply the reciprocal of the transverse relaxation time, T_2. In order to validate the liquid-metal microcoil results, we compare the results with the R_2 measured with a conventional solenoid type coil (3 turns, 900 μm inner diameter).

Fig. 4 shows the experimental results for the hematocrit-R_2 characterization curve measured with both the liquid-metal microcoil and the conventional solenoid type coil. The two experiments were carried out on two separate occasions and with blood

samples from two different individuals. Each measurement is repeated 5 times and the standard deviation is used as an estimation for the measurement error in R_2. Indeed, the results obtained by both types of coil agree well with each other. The transverse relaxation rate, R_2 increases quadratically with the hematocrit level of the

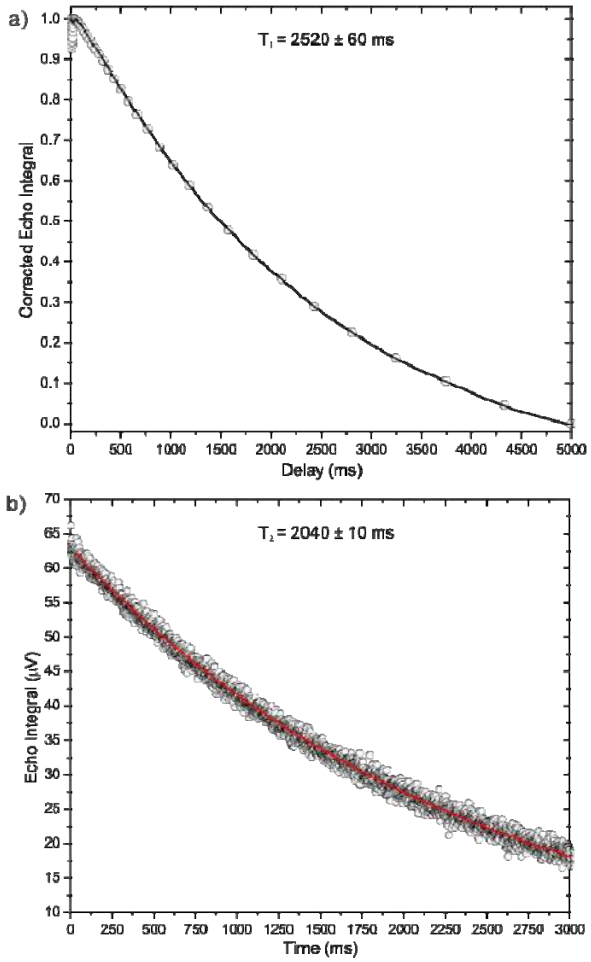

Figure 3 : (a) T_1 measurement: the corrected echo integral collected with a standard inversion-recovery CPMG pulse sequence for DI-water. The T_1 relaxation time for DI-water is 2520 ± 60 ms. (b) T_2 measurement: the echo integral collected with CPMG pulse trains. The T_2 relaxation time for DI-water is 2040 ± 10 ms.

blood sample.

The polynomial fit for the quadratic curve (Matlab, MathWorks, USA) is as follows:

$$R_2 \approx 5.17 Hct^2 + 5.42 Hct + 0.604, \tag{3}$$

where Hct is the fraction of hematocrit level. The goodness of fit, R^2 of the quadratic polynomial curve is 0.9922. The results are consistent with the finding of Spees et. al.[37], where they studied the relationship between R_2 with the blood oxygen

saturation at 30% and 40% hematocrit level, respectively. They found that the R_2 at 40% hematocrit is higher than blood sample at 30% hematocrit level. The volume magnetic susceptibility of blood, χ_{blood} is given by:[37]

$$\chi_{\text{blood}} = -0.722\times10^{-6} + Hct[0.26(1-Y)-0.014]\times10^{-6}, \quad (4)$$

where Y is the fraction of oxygenated hemoglobin. From equation (4), the magnetic susceptibility of blood increases with the hematocrit for a constant oxygenation level. Therefore, with more red blood cells at higher hematocrit level, the transverse relaxation rate of the blood sample is enhanced due to higher magnetic susceptibility. Oxygenated red blood cell (oxyhemoglobin) is diamagnetic since it has no unpaired electrons due to its covalent bonds.[38]

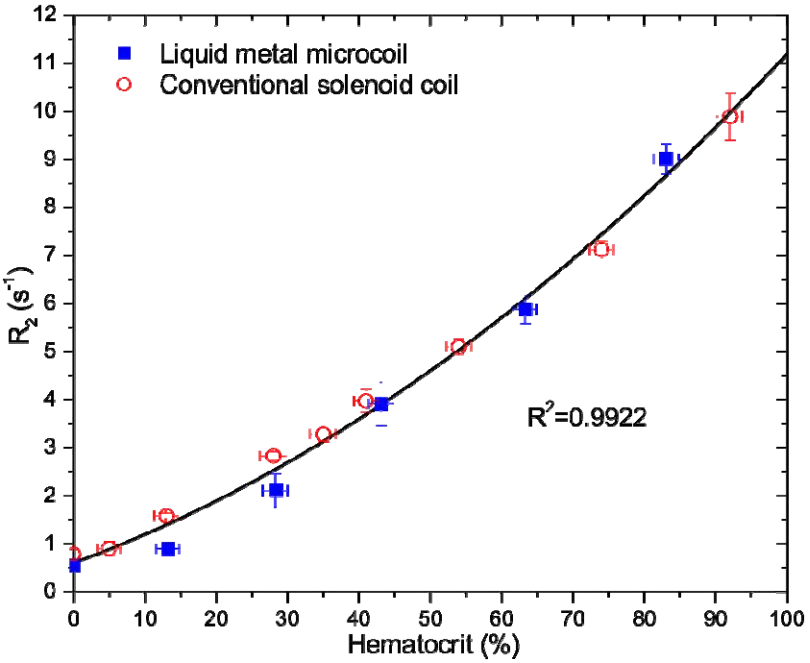

Figure 4 : Hematocrit-R_2 characterization curve for human red blood cell sample. The data obtained by the liquid-metal microcoil and the conventional solenoid type coil are in good accordance to each other. R_2 increases quadratically with the hematocrit level of the blood.

4. Conclusions

In conclusion, we have demonstrated the fabrication and characterization of an adhesive-based liquid-metal microcoil for magnetic resonance relaxometry measurement. The technique proposed in this paper - lamination of laser cut dry adhesive sheets offers a convenient way to fabricate three-dimensional microcoils without considerable fabrication efforts and the need of incurring high fabrication cost. The liquid-metal microcoil can readily be integrated with the sample chamber for realizing a lab-on-a-chip platform for MRR measurements. The sample chamber can be disposed off simply by

removing the protective film between the coil and sample adhesive layers. This concept ensures that there is no cross contamination between different samples and without the need to clean the sample chamber before every measurement. The same microcoil could be reused for multiple measurements. From the microcoil characterization experiments, the ability of liquid-metal microcoil for performing MRR measurements was demonstrated. The results obtained from the microcoil for the parametric study of the hematocrit-R_2 relationship agree well with the data obtained with the conventional solenoid-type coil. In addition, the ability of the microcoil in detecting a subtle change in the blood hematocrit level could open the door for the development of portable MRR device to aid the diagnosis of anemia caused by the low number of red blood cells. In the future work, the adhesive-based liquid-metal microcoil could be integrated onto a flexible electronic patch for noninvasive in-vivo MRR detection in human.

5. Acknowledgement

This work is supported by Singapore - MIT Alliance for Research and Technology (SMART) Centre, BioSystems and Micromechanics (BioSyM) IRG, Singapore.

References

1 T. F. Kong, H. S. E, H. S. Sugiarto, H. F. Liew, X.Wang,W. S. Lew, N.-T. Nguyen and Y. Chen, Microfluid Nanofluid, 2010, 10, 1069–1078.

2 J.-W. Choi, C. H. Ahn, S. Bhansali and H. T. Henderson, Sens. Actuators. B, 2000, 68, 34–39.

3 M. A. M. Gijs, Microfluid Nanofluid, 2004, 1, 22–40.

4 C. Massin, F. Vincent, A. Homsy, K. Ehrmann, G. Boero, P. A. Besse, A. Daridon, E. Verpoorte, N. F. de Rooij and R. S. Popovica, J. Magn. Reson., 2003, 164, 242–255.

5 A. M.Wolters, D. A. Jayawickrama and J. V. Sweedler, Curr. Opin. Chem. Biol., 2002, 6, 711–716.

6 C. Massin, G. Boero, F. Vincent, J. Abenhaim, P. A. Besse and R. S. Popovic, Sens. Actuators A Phys., 2002, 97-98, 280–288.

7 C. Y. Hsieh, Y. T. Yeh and L. S. Fan, Microsyst. Technol., 2011, 17, 1311–1317.

8 P. van Bentum, J. Janssen, A. Kentgens, J. Bart and J. Gardeniers, J. Magn. Reson., 2007, 189, 104–113.

9 Y. Maguire, I. L. Chuang, S. Zhang and N. Gershenfeld, Proc. Natl. Acad. Sci., 2007, 104, 9198–9203.

10 V. Badilita, K. Kratt, N. Baxan, M. Mohmmadzadeh, T. Burger, H.Weber, D. v. Elverfeldt, J. Hennig, J. G. Korvinkcd and U.Wallrabead, Lab Chip, 2010, 10, 1387–1390.

11 N. Sun, T.-J. Yoon, H. Lee,W. Andress, R.Weissleder and D. Ham, IEEE J. Solid-State Circuits, 2011, 46, 342–352.

12 D. Issadore, C. Min, M. Liong, J. Chung, R. Weissleder and H. Lee, Lab Chip, 2011, 11, 2282–2287.

13 H. Lee, E. Sun, D. Ham and R.Weissleder, Nat. Med., 2008, 14, 869–874.

14 J. B. Haun, C. M. Castro, R.Wang, V. M. Peterson, B. S. Marinelli, H. Lee and R. Weissleder, Sci. Transl. Med., 2011, 3, 71ra16.

15 W. K. Peng, A. A. S. Bhagat and J. Han, to be published, 2011.

16 W. K. Peng, A. A. S. Bhagat and J. Han, in Biomedical Engineering Society Annual Meeting, Hartford, 2011.

17 W. K. Peng, A. A. S. Bhagat and J. Han, in Experimental Nuclear Magnetic Resonance Conference, Pacific Grove, 2011.

18 D. Golda, J. H. Lang and M. L. Culpepper, J. Microelectromech. Syst., 2008, 17, 1537–1545.

19 N.-T. Nguyen, K. M. Ng and X. Huang, Appl. Phys. Lett., 2006, 89, 052509.

20 A. Beyzavi and N. T. Nguyen, J. Micromech. Microeng., 2008, 18, 095018.

21 J. A. Rogers, R. J. Jackman, G. M. Whitesides, D. L. Olson and J. V. Sweedler, Appl. Phys. Lett., 1997, 70, 2464–2466.

22 L. O. Sillerud, A. F. McDowell, N. L. Adolphi, R. E. Serda, D. P. Adams, M. J. Vasile and T. M. Alam, J. Magn. Reson., 2006, 181, 181–190.

23 A. C. Siegel, D. A. Bruzewicz, D. B. Weibel and G. M. Whitesides, Adv. Mater., 2007, 19, 727–733.

24 J.-H. So, J. Thelen, A. Qusba, G. J. Hayes, G. Lazzi and M. D. Dickey, Adv. Funct. Mater., 2009, 19, 3632–3637.

25 S. Cheng and Z. Wu, Lab Chip, 2010, 10, 3227–3234.

26 C.-Y. Wu, W.-H. Liao and Y.-C. Tung, Lab Chip, 2011, 11, 1740–1746.

27 J.-H. So and M. D. Dickey, Lab Chip, 2011, 11, 905–911.

28 Ryan, C. Chiechi, E. A. Weiss, M. D. Dickey and G. M. Whitesides, Angew. Chem.

Int. Ed., 2007, 47, 142–144.

29 M. H. C. Lam, M. A. Homenuke, C. A. Michal1 and C. L. Hansen, J. Micromech. Microeng., 2009, 19, 095001.

30 A. G. Webb, Prog. Nucl. Mag. Res. Sp., 1997, 31, 1–42. 31 F. Casanova, J. Perlo and B. Bl¨umich, Single-Sided NMR, Springer, Germany, 1st edn, 2011, p. 59.

32 H. A. Wheeler, Proc. Inst. Radio Engrs., 1928, 16, 1398–1400.

33 M. A. Brown and R. C. Semelka, MRI basic principles and applications, Wiley, North Carolina, 3rd edn, 2003, pp. 21–31.

34 L. Harder and L. Boshkov, Crit. Care Clin., 2010, 26, 335–354.

35 W. Secomski, A. Nowicki, F. Guidi, P. Tortoli and P. A. Lewin, J. Ultrasound Med., 2003, 22, 375–384.

36 N. V. Iftimia, D. X. Hammer, C. E. Bigelow, D. I. Rosen, T. Ustun, A. A. Ferrante, D. Vu and R. D. Ferguson, Opt. Express, 2006, 14, 3377–3388.

37 W. M. Spees, D. A. Yablonskiy, M. C. Oswood and J. J. Ackerman, Magn. Reson. Med., 2001, 45, 533–542.

38 M. Zborowski, G. R. Ostera, L. R. Moore, S. Milliron, J. J. Chalmers and A. N. Schechter, Biophys J., 2003, 84, 2638–2645.